V Workshop "Estallidos de Formación Estelar en Galaxias“
Star Formation and Metallicity

Granada, 28 February – 2 March 2007

3D Spectroscopy of Wind Driven Nebulae: The Large Western Knot in the Halo of NGC 6543



David Martín-Gordón[1]

José M. Vílchez[1], Angels Riera[2,3]



(1) Instituto de Astrofísica de Andalucía, CSIC, Granada – Spain.

(2) Departament de Física i Enginyeria Nuclear, Universitat Politècnica de Catalunya, Vilanova i la Geltrú – Spain.

(3) Department d'Astronomia i Meteorologia, Universitat de Barcelona, Barcelona – Spain.

Aims of this work (I)

The history of stellar winds and ejecta is written in the extended wind-driven nebulae around massive (WRN) and intermediate mass stars (PNe). Fast winds can produce shock excitation of the interstellar medium in the haloes of PNe and WR nebulae providing an extra source of heating for their thermal balance.

We are performing an observational program aimed to evaluate the realistic impact on the interstellar medium of these effects. A search for possible footprints of shock-heated gas in the extended haloes of wind-driven nebulae has been carried out using deep multi-filter imaging of a sample of WRN and PNe nebulae.

The comparison of the emission of different states of ionization or different emission conditions provides a direct evidence for fine-scale structure within the halo of the nebula . Subsequently, 3D spectroscopy has been performed for those locations of the nebulae which are candidate to host an extra heating contribution as indicated by our previous 2D ionization structure maps.

Aims of this work (II)

In this work, as an example, we present new results of 3D spectroscopy taken with the PMAS/PPAK Instrument (Calar Alto Observatory, Spain) for the halo of the candidate nebula NGC 6543. The large western knot in the halo of this young planetary nebula is an excellent place to derive new spectroscopic constrains in order to evaluate the role of photo-ionization as the main excitation mechanism.

The Sample I - Imaging

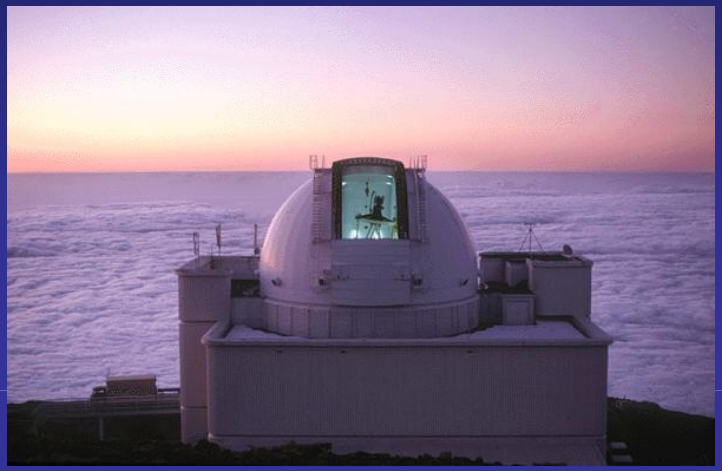
OBJECT	RA	Dec	Type	Instrument	Filters
G2.4+1.4	17:45:47.00	-26:10:29.0	WR-ring	INT-WFC	Hα, [OII], [OIII],[SII], B, r, g
M1-67	19:11:30.89	+16:51:38.1	WR-ring	CAHA 2.2-BUSCA	Hα, Hβ, [NeIII], [OIII], [SIII], V, b, y, I
M1-67	19:11:30.89	+16:51:38.1	WR-ring	INT-WFC	Hα, [OII], [OIII], [SII], B, r
NGC2359	07:18:29.09	-13:13:01.5	WR-ring	INT-WFC	Hα, [OII], [OIII], [SII], r, g
NGC246	00:47:03.34	-11:52:19.0	Pn-halo	CAHA 2.2-BUSCA	Hα, [NeIII], [OIII], [SIII], V, b, y, I
NGC6210	16:44:29.00	+23:48:00.0	Pn-halo	CAHA 2.2-BUSCA	Hα, Hβ, [NeIII], [OIII], [SIII], V, b, y, I
NGC6543	17:58:33.40	+66:37:58.9	Pn-halo	INT-WFC	Hα, [OII], [OIII], [SII], B, r, g
NGC6720	18:53:35.00	+33:01:43.0	Pn-halo	CAHA 2.2-BUSCA	Hα, Hβ, [NeIII], [OIII], [SIII], V, b, y, I
NGC6804	19:11:31.00	+09:13:31.0	Pn-halo	CAHA 2.2-BUSCA	Hα, Hβ, [NeIII], [OIII], [SIII], V, b, y, I
NGC6826	19:44:48.00	+50:31:30.0	Pn-halo	CAHA 2.2-BUSCA	Hα, [NeIII], [OIII], [SIII], V, b, y, I
NGC6888	20:12:26.90	+38:21:17.6	WR-ring	INT-WFC	Hα, [OII], [OIII], [SII], B, r, g
NGC6891	20:15:09.00	+12.42.17.0	Pn-halo	CAHA 2.2-BUSCA	Hα, [NeIII], [OIII], [SIII], V, b, y, I
NGC6894	20:16:24.00	+30:33:54.0	Pn-halo	CAHA 2.2-BUSCA	Hα, [NeIII], [OIII], [SIII], V, b, y, I
NGC7009	21:04:11.0	-11:21:50.0	Pn-halo	CAHA 2.2-BUSCA	Hα, [NeIII], [OIII], [SIII], V, b, y, I
NGC7662	23:25:53.99	+42:32:06.0	Pn-halo	INT-WFC	Hα, [OIII], r, g
NGC7662	23:25:54.00	+42:32:06.0	Pn-halo	CAHA 2.2-BUSCA	Hα, Hβ, [NeIII], [OIII], [SIII], V, b, y, I
S308	06:50:50.90	-23:49:14.0	WR-ring	INT-WFC	Hα, [OII], [OIII], [SII], r, g

The Sample II - 3D spectroscopy

OBJECT	RA	Dec	Type	Gratings	Pointings
M1-67	19:11:30.89	+16:51:38.1	WR-ring	V300	2
NGC6543	17:58:33.40	+66:37:58.9	Pn-halo	R1200 & V300	4
NGC6888	20:12:26.90	+38:21:17.6	WR-ring	R1200 & V300	4
NGC7662	23:25:53.99	+42:32:06.0	Pn-halo	V300	3

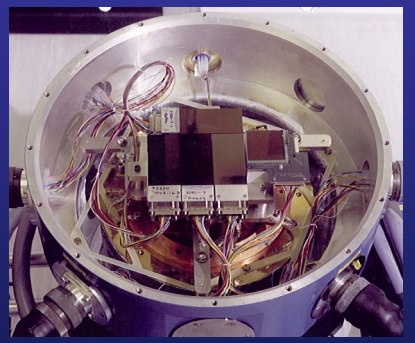
Observations: Telescopes and instruments (I)

INT Telescope



- Located in ORM (La Palma)
- 2.5 m diam. primary mirror

Wide Field Camera (WFC)

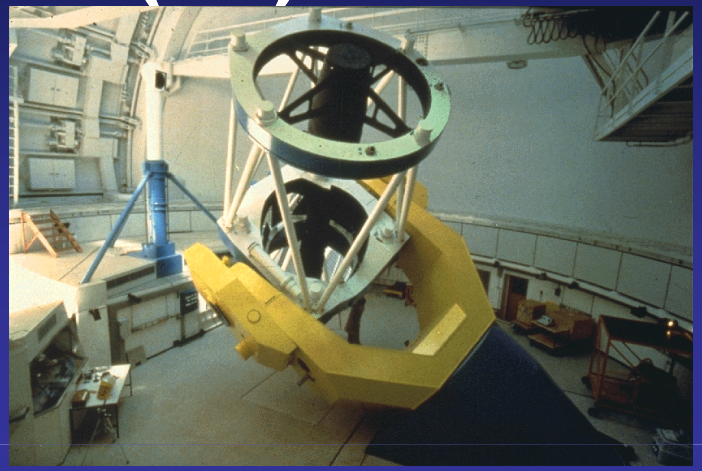


- 4 CCD's mosaic
- Pixel size – 13.5 μm x 13.5 μm
- Pixel scale – 0.333 arcsec / píxel
- Field of view – 34 arcmin x 34 arcmin
- Working temperature – 153 K

Observations: Telescopes and instruments (II)

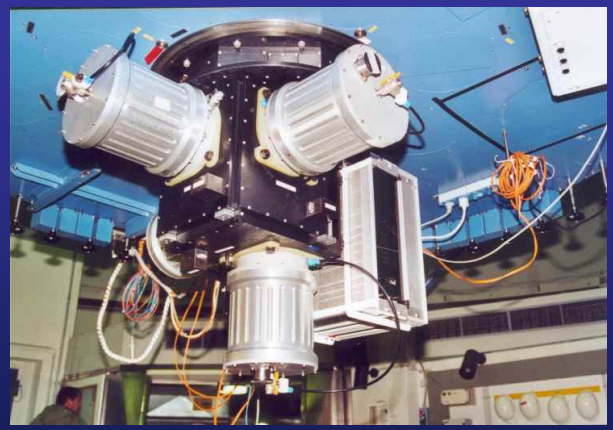
2.2m-CAHA Telescope

- Located in CAHA (Calar Alto, Almeria)
- 2.2 m diam. primary mirror



BUSCA Camera

- CCD camera system which allows simultaneous direct imaging of the same sky area in four colors
- 3 CCD's (4096 x 4096 pixels), frontside devices and 1 CCD backside thinned (in the uv channel).
- Pixel size – 15 μm x 15 μm
- Pixel scale – 0.176 arcsec / píxel
- Field of view – 12 arcmin x 12 arcmin



Observations: Telescopes and instruments (III)

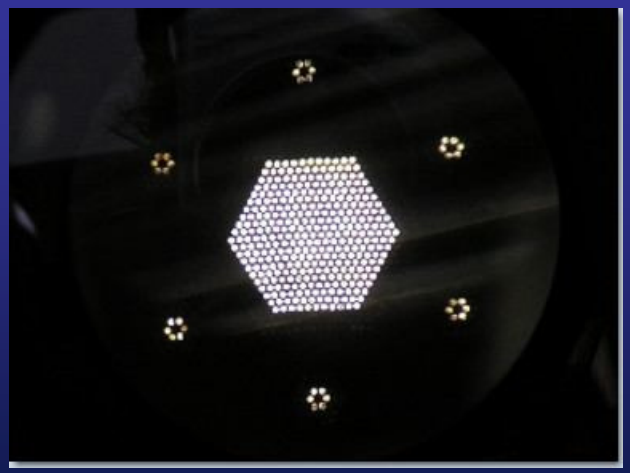
3.5m-CAHA Telescope

- Located in CAHA (Calar Alto, Almeria)
- 3.5 m diam. primary mirror



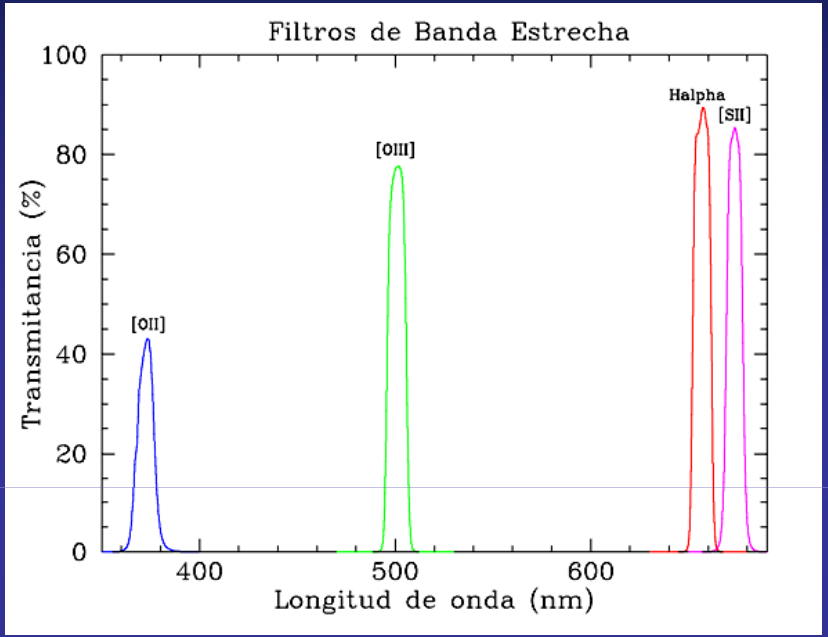
PMAS/PPAK Spectrograph

- 331 densly packed optical fibers
- Spatial sampling - 2.7 arcseconds per fiber
- Field of view – 74 arcsec x 65 arcsec



Observations: Filters

- Narrow band filters.
- Hα narrow band filter contains [NII] line.



Filter	λ (Å)	Δλ (Å)
Hα	6568	95
[OIII]	5008	100
[OII]	3727	100
[SII]	6725	80

Observations: Gratings

- High and low resolution gratings.

Grating	λ_1 (Å)	λ_2 (Å)	FWHM (Å)
R1200	6212	6871	~2.77
R1200	4322	5061	~2.77
R1200	3663	4428	~2.76
V300	3701	7102	~10.7

Data Reduction - Imaging

- Bias correction
- Flat field correction
- Astrometry
- Fotometry in narrow band filters

Data Reduction – 3D Spectroscopy

- Find the position of the spectra in the raw frame
- Trace the position of the spectra along the spectral direction
- Extract the spectra
- Correct for the distortion & dispersion
- Fiber-to-fiber transmission correction
- Calibration with standard stars
- Creation of datacubes with dithering technique

Data Analysis – 3D Spectroscopy

- 990 spectrums on dithering datacubes.
- A procedure has been designed to perform flux measurement, including continuum subtraction and error calculation.
- Maps have been obtained measuring the flux of the selected emission line in all of the spectrums of each datacube.

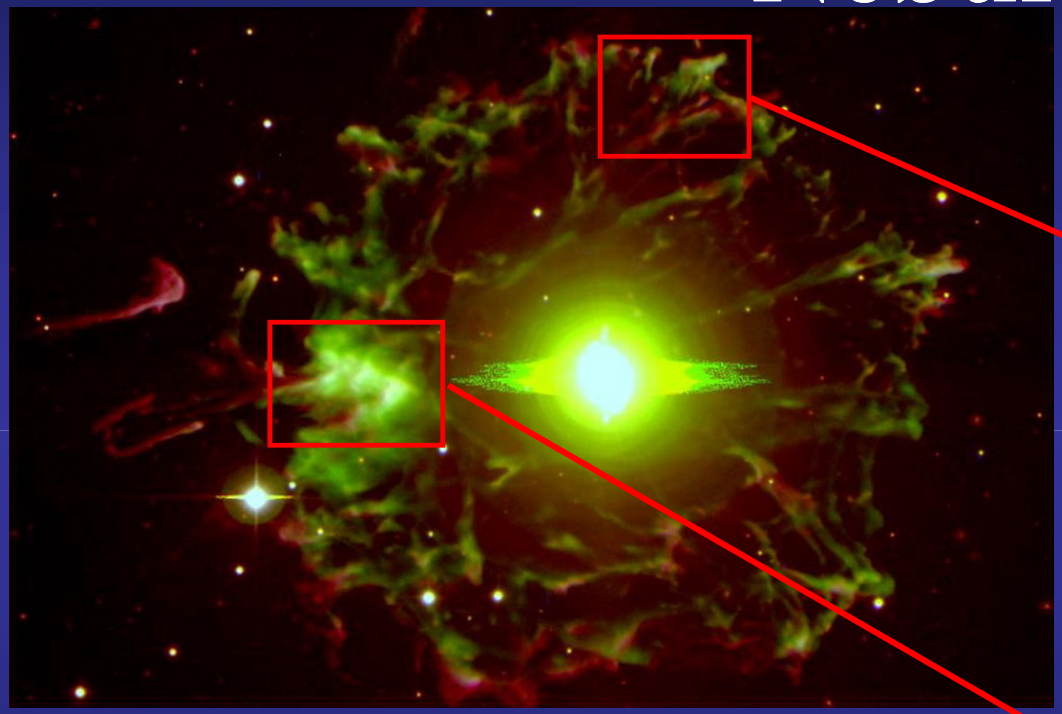
The Halo of the NGC6543 Nebula

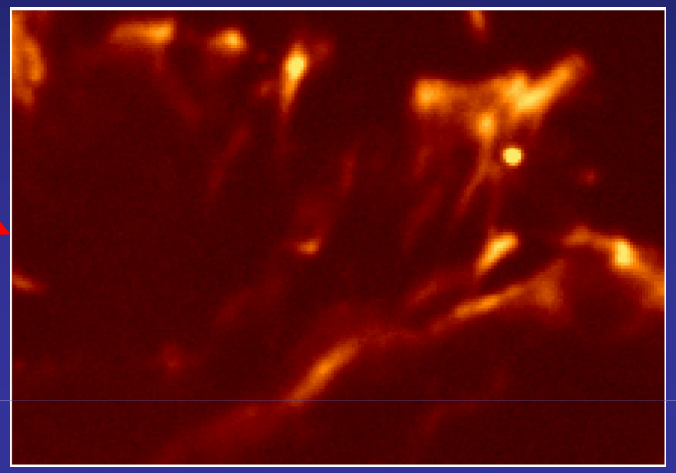
NGC6543 is a typical example of a well known planetary nebula with an extended ionized halo (e.g. Manchado & Pottasch 1989; Luridiana et al. 2003). Here we do not present a study of the central parts of this well known nebula, but we are interested in the ionization of selected faint filamentary structures and knots detected in its halo.

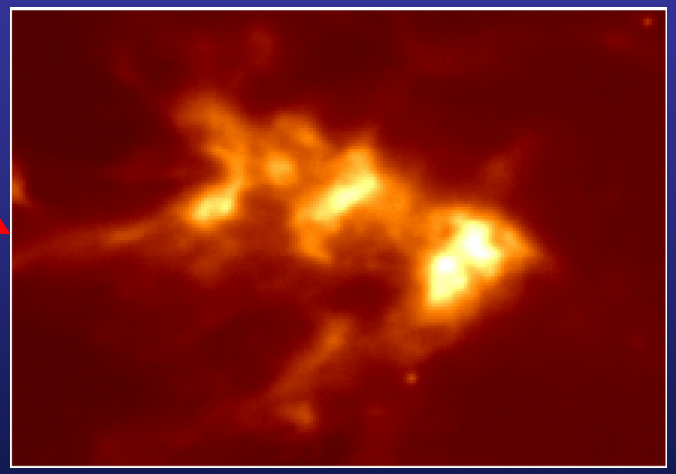
It has been claimed that the haloes of some multiple shell PNe, and in particular in the case of NGC 6543, are much hotter than their respective core nebulae (e.g. Manchado & Potasch 1989; Meaburn et al. 1991; Middlemass et al.1989, 1991).Middlemass et al. (1989) have shown that photoelectric heating is not able to reproduce the high temperatures observed in the halo of NGC 6543, claiming that an extra heating source would be required.

A candidate for this extra energy source is the fast wind passing the cold filamentary knots observed in the haloes of this Planetary Nebula.

The Halo of the NGC6543 Nebula







The composite image of NGC 6543 made with the Hα + [NII] (Red), [OIII] (Green) and [OII] (Blue) emission line images displayed with linear intensity.

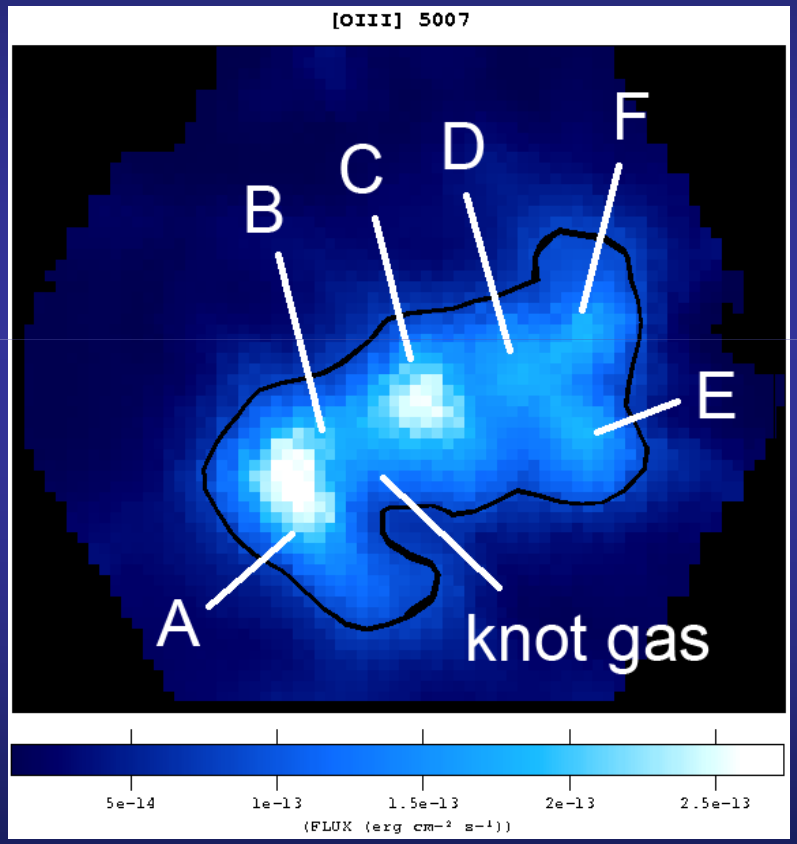
This false-color image is made of three (RGB) 8-bit image. This image shows the fine-scale structures of the halo.

Diffuse Gas Surrounding the Knot

Recently Mitchell et al (2005) have studied the kinematics of the large Western knot of the halo of NGC 6543. They have concluded that there exist gas flows around the otherwise kinematically inert knot. This gas developing velocities comparable to the sound speed as the gas is photo-evaporated off the ionized surface. No evidence is found for the knot being interacting with a fast wind, suggesting that this knot structure was not a product of instabilities in the interface between the fast and the asymptotic giant branch winds.

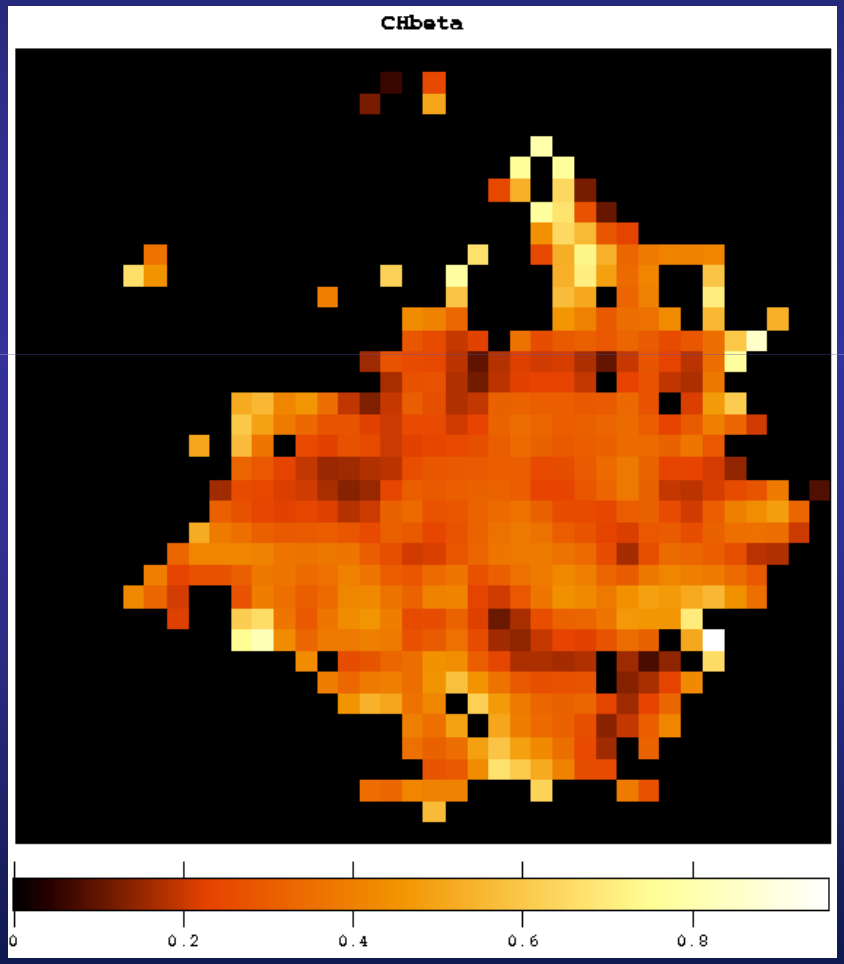
A scenario was proposed in which the knot is embedded in a slowly expanding red giant wind whereas its surface is photo-ionized by the central PNe star. We have detected spectroscopically this gaseous component, thus discriminating the physical properties of the brighter sub-knots structure across the knot with respect to this low surface brightness gaseous envelope.

[OIII] Flux



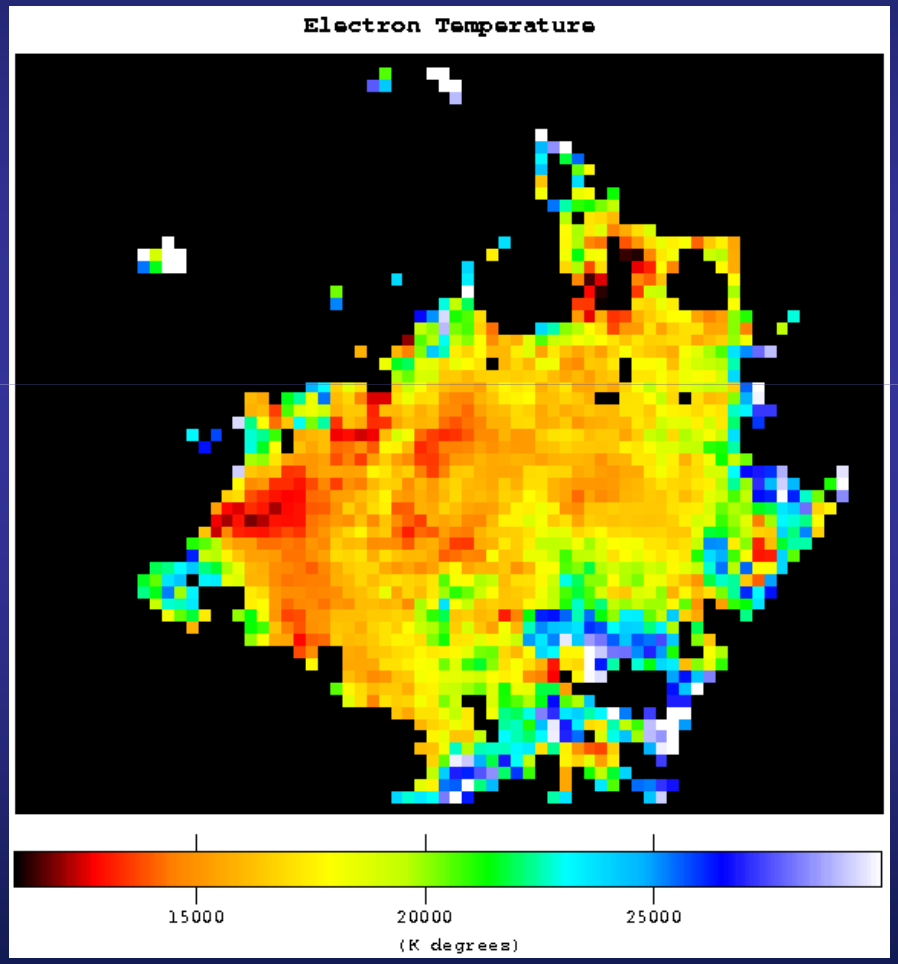
This map shows the flux of the 5007 [OIII] line in units of erg cm^{-2} s^{-1}. The continuos line delineates the isocontour corresponding to 8 10^{-14} flux. The sub-knots marked on the map as well as the boundary of the knot gas refers to the same features identified in Mitchell et al (2005). North is down and West is right.

Reddening Coefficient $C(H_\beta)$



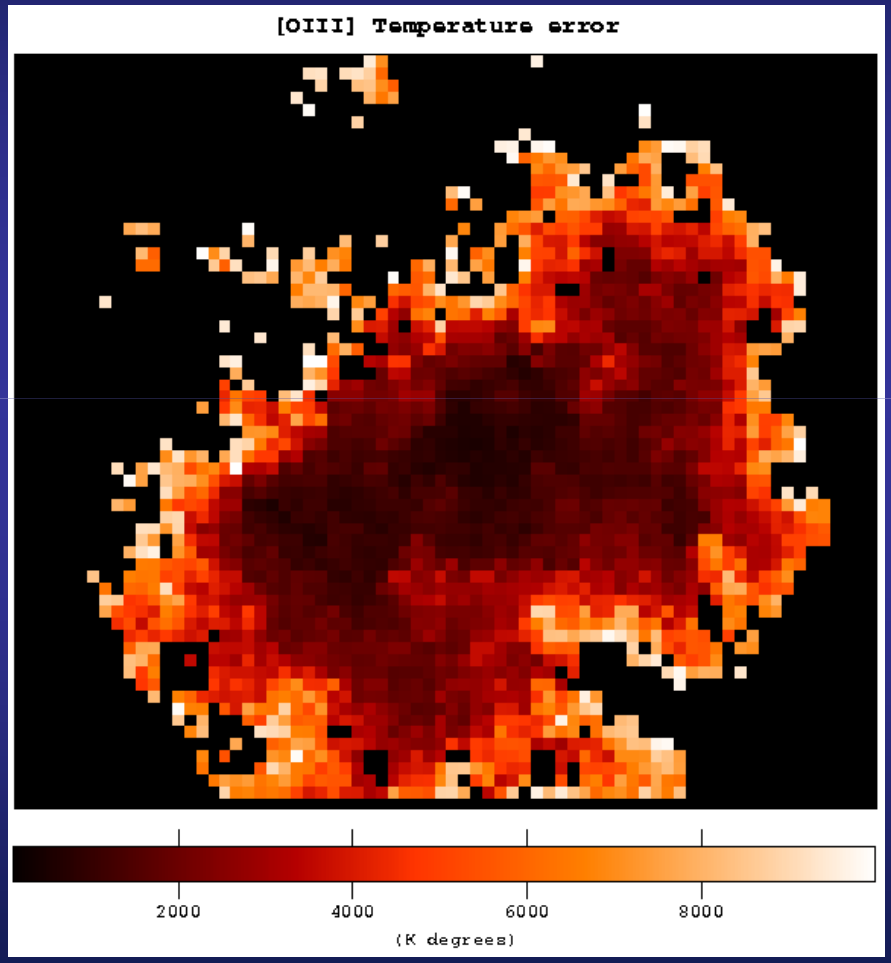
Map of the reddening coefficient, $C(H_\beta)$, derived from the H_α/H_β ratio assuming case B recombination for a low density and an average T_e of $1.5\ 10^4$ K.

Electron Temperature T_e



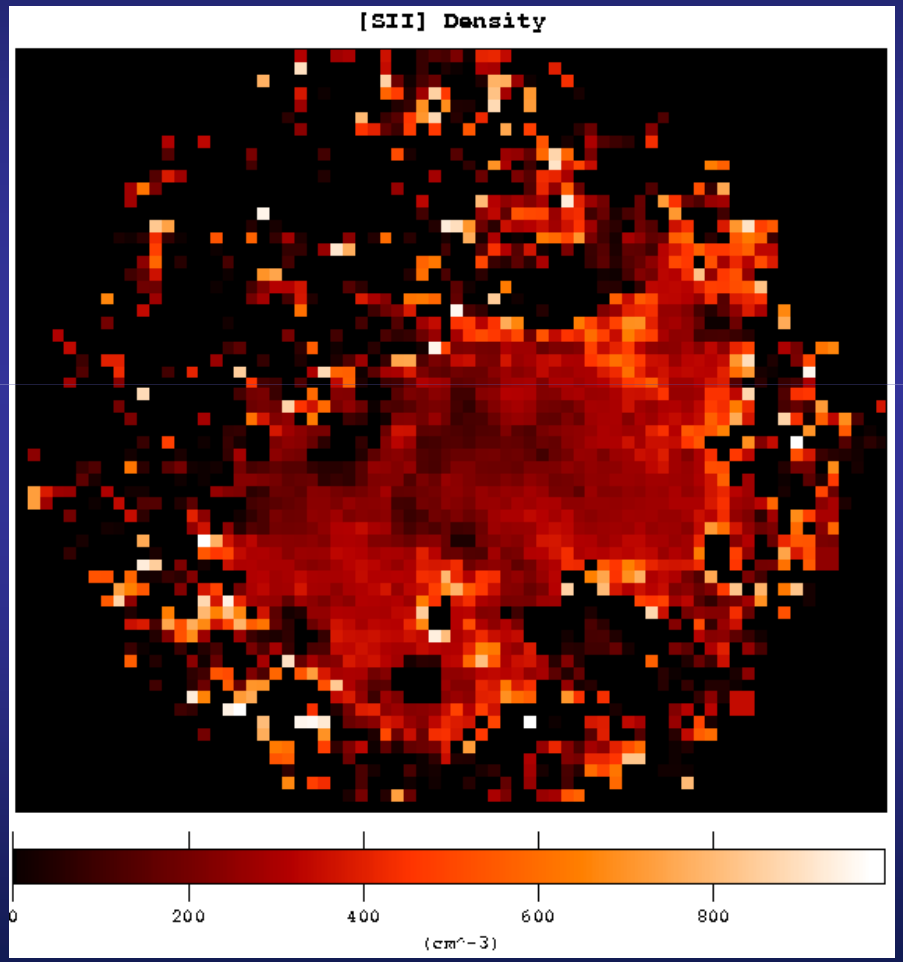
The electron temperature, T_e, map derived from the ratio of the (CEL) lines [OIII]4363/(4959+5007). Electron temperatures show a substantial variation across the whole structure. T_e values tend to be lower (~1.4 10^4 K) in the brighter sub-knots, though some slight shifts between both [OIII] flux and T_e *extrema* are noticeable. On the other hand, the tenuous gas embedding the knots appears much hotter, reaching values of order 2 10^4 K.

Electron Temperature Error



Error map of the [OIII] temperature, T_e, This error was calculated from the signal/noise ratio obtained for each individual [OIII] line flux measurement.

Density



Map of the density in the single ionized zone obtained from the [SII]6717/6731 ratio. The field covered by the data is of ~1 arcmin in diameter and the final spatial resolution achieved is 1 arcsec. The density values derived range from the low density limit up to ~ 600 cm-3 ; though some degree of structure is apparent, the higher density zones do not follow the knots/structure seen in the [OIII] flux map; however, this density map shows a much closer relation with the electron temperature distribution.

- A gaseous envelope around the knot has been detected and measured using 3D spectroscopy.
- Density values range from the low density limit up to ~600 cm^{-3}.
- Electron temperature shows conspicuous variations, with values going from 1 to 2.5 10^4 K. The mean T_e=1.82 10^4 K, mode T_e= 1.63 10^4 K and standard deviation of 0.37 10^4 K.
- The diffuse gaseous envelope appears to be hotter and more dense than the sub-knots.
- The average reddening is low, presenting a smooth spatial distribution with some degree of small scale estructure.

Future Work

- Detailed analysis of results for the sample (in progress)
- Comparison between observed ionization structure and:
  - Photoionization models
  - Hidrodynamic simulations
  - Theoretical models.
- Wavelets Analisys (in progress)